Macromolecules

pubs.acs.org/Macromolecules Article

Phase Behavior of Linear-Bottlebrush Block Polymers

Lucy Liberman, McKenzie L. Coughlin, Steven Weigand, Frank S. Bates,* and Timothy P. Lodge*

Cite This: *Macromolecules* 2022, 55, 2821−2831 Read Online

ACCESS | Metrics & More | Article Recommendations | Supporting Information

ABSTRACT: Block copolymers (BCPs) self-assembled into 3D network phases are promising for designing useful materials with multiple properties that rely on domain continuity. However, access to potential applications has been limited because network formation with linear BCPs tends to occur only over narrow compositional windows. Another constraint is slow self-assembly kinetics at higher molecular weights, which limits the network unit cell dimensions and the resulting material properties. Architecturally asymmetric, linear-bottlebrush BCPs have previously been demonstrated to promote self-assembly into complex micellar phases. The architectural asymmetry has been demonstrated to induce favorable curvature toward the linear block. However, linear-bottlebrush copolymer phase behavior and self-assembly into network phases have not been systematically studied. Here, we map the phase behavior of eight sets of diblock polymers with a linear-bottlebrush architecture in the expected vicinity of the double-gyroid phase. We demonstrate the effects of architectural asymmetry and the linear block cohesive energy density on self-assembly into double-gyroid, lamellar, and hexagonal phases. Through a combination of molecular and structural characterization techniques, we demonstrate that the shape of the polymer and the identity of the linear block provide significant control over the molecular factors that dictate network formation.

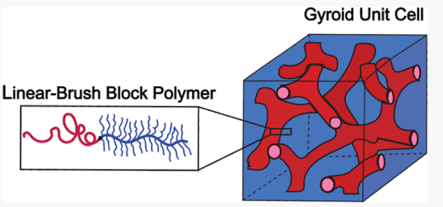

INTRODUCTION

Diblock copolymer melts microphase separate and self-assemble into diverse periodic nanostructures, such as spherical micelles, hexagonally packed cylinders, lamellae, and three-dimensional networks.[1] The resulting nanostructure is mainly dictated by the volume fraction of one block (f) and the segregation strength between the two blocks (χN), where χ is the Flory−Huggins segment−segment interaction parameter and N is the total degree of polymerization.[2] Several network phases have been identified in BCPs, such as the cubic double-gyroid, double-diamond, orthorhombic *Fddd*, and double-primitive.[3−9] However, theoretical calculations demonstrate that only *Fddd* and double gyroid are thermodynamically stable in diblock polymer melts, with double gyroid having the larger stability window.[10−12]

The double-gyroid network phase is composed of periodic interpenetrating domains, where the bicontinuity has been shown to provide the material with advanced mechanical properties.[13−15] Since their discovery in BCPs,[16] network phases have attracted scientific interest because of the opportunity to incorporate orthogonal properties in one material, for example, mechanical strength and ion conduction,[3] through the careful selection of the constituent blocks. The ability to combine several characteristics in one material is appealing, but access to potential applications has been limited, in part because network phases tend to be stable only over narrow compositional windows.[1] This constraint has been attributed to packing frustration, caused by the curvature variation around the network multinode connectors.[10,17] Another limiting factor is the slow self-assembly kinetics at high molecular weights for linear diblocks, which places an upper boundary on the tractable molecular size and hence the accessible pore size of the network structures and the resulting mechanical properties of the matrix.[11] A potential approach to overcoming both of these challenges is to deviate from the conventional linear−linear diblock molecular structure through the introduction of architectural asymmetry in the form of bottlebrush blocks, which produce differences in the shape and space-filling characteristics of the macromolecule. (Here, "linear" refers to a flexible polymer chain with side groups that are not significantly longer than the backbone spacing between the pendant units.) Self-consistent-field theory (SCFT) calculations indicate that architectural asymmetry in diblock polymers distorts the phase diagrams and shifts the network windows as a function of block volume fraction.[18−24] Here, we have experimentally investigated how architectural asymmetry in linear-bottlebrush diblock copolymers affects phase behavior, with a focus on the network-forming region.

Bottlebrush polymers are composed of a linear backbone with densely grafted side chains that are significantly longer than their backbone spacing. Steric repulsion between the side chains induces an extended backbone conformation; the lateral "thickness" of the chains reduces the entanglement density.[25,26] Introduction of a polymer block with a bottlebrush architecture creates architectural asymmetry, including conformational

Received: February 15, 2022
Revised: March 10, 2022
Published: March 29, 2022

https://doi.org/10.1021/acs.macromol.2c00337
Macromolecules 2022, 55, 2821−2831

asymmetry, in a linear-brush diblock. The architecture of the brush block can be controlled by the length and/or the grafting density of the side chains, while the conformation is determined by the statistical segment length of the resulting brush.

Several experimental studies reported that Janus and gradient bottlebrush block polymers can self-assemble into a double gyroid.[27−29] However, previous work on the phase behavior of linear-bottlebrush diblock polymers has primarily focused on nanoparticle-based Frank-Kasper phases.[30,31] Recent SCFT computational work by Park et al.[22] has specifically studied the stability of the double-gyroid network in brush-based diblock polymers and predicts that linear-bottlebrush polymers have stable gyroid regions. When the linear block is in the minority domain, increasing architectural asymmetry shifts the phase boundaries to higher linear block compositions, without significantly changing the size of the double-gyroid window.[22] However, experimental work on the self-assembly of linear-brush polymers into network phases is limited.

Here, we use ring-opening metathesis polymerization (ROMP) to synthesize linear-bottlebrush polymers. ROMP is a controlled living polymerization technique, which can provide excellent control over the size and the architecture of the desired polymer, while producing very low molecular-weight dispersities.[32−34] Furthermore, ROMP is quite rapid, which allows the synthesis of libraries of polymers in a short time, thus providing the opportunity to efficiently explore several parameters of interest. We report a systematic study of the phase behavior of over 250 linear-bottlebrush diblock copolymers with varying composition, molecular weight, architectural asymmetry, and linear block polarity, centered on the double gyroid. By a combination of molecular and structural characterization methods, we show that the architecture and the linear block polarity exert significant control over the compositions, compositional window size, and the molecular weights available for network formation.

EXPERIMENTAL SECTION

Materials. *cis*-5-Norbornene-*endo*-2,3-dicarboxylic anhydride was obtained from TCI Chemicals. Farnesol was obtained from Sigma-Aldrich; phytol was purchased from ApexBio; solanesol was acquired from Cayman Chemical Company. SiliCycle Inc. SiliaBond DMT was obtained from Fischer Scientific. Palladium (10%) on activated carbon, second-generation Grubbs' catalyst, 4-dimethylaminopyridine, *N*-(3-dimethylaminopropyl)-*N*′-ethylcarbodiimide hydrochloride, anhydrous methanol, anhydrous dichloromethane, isoamyl alcohol, and pyridine were purchased from Sigma-Aldrich. Dichloromethane for ring-opening metathesis polymerization was obtained from a solvent purification column and used inside a glovebox. Deuterated chloroform and benzene-d_6 for ^{1}H NMR spectroscopy were purchased from Cambridge Isotopes. TZero and standard hermetic aluminum pans for small-angle X-ray scattering (SAXS) and differential scanning calorimetry (DSC) analysis were obtained from DSC Consumables, Inc.

Synthesis. Homopolymers and a total of 258 diblock copolymers were synthesized using sequential ROMP using Grubbs' third-generation catalyst, which was prepared from the second generation, as described in the Supporting Information. The linear-block volume fraction for each polymer was determined using ^{1}H NMR spectroscopy and estimated block densities (see the Supporting Information), while the number-average molecular weight (M_n) and dispersity ($Đ$) were established using size-exclusion chromatography with multiangle light-scattering detection (SEC-MALS). Detailed descriptions of the monomer and polymer synthesis, along with characterization data, are provided in the Supporting Information.

^{1}H NMR Spectroscopy. Chemical structural information for the monomers and polymers was obtained using proton nuclear magnetic resonance spectroscopy (^{1}H NMR) in $CDCl_3$ and in benzene-d_6 for Grubbs' third-generation catalyst. ^{1}H NMR spectra were collected on a 400 MHz (Bruker Avance III HD Nanobay AX-400) spectrometer using 16−128 scans. Representative ^{1}H NMR data are provided in the Supporting Information.

SEC-MALS. Polymer solutions in tetrahydrofuran (THF) were prepared at a concentration of ∼5 mg/mL, filtered through 0.22 μm polytetrafluoroethylene syringe filters, and examined by SEC-MALS with THF as the mobile phase. 50 μL of each solution was injected into the instrument, equipped with a Tosoh Styragel guard column, and three sequential columns packed with 5 μm styrene-divinylbenzene particles. The weight-average molecular weight (M_w), number-average molecular weight (M_n), and dispersity ($Đ = M_w/M_n$) were determined using a Wyatt Technology DAWN Heleos II 18-angle light-scattering detector at a wavelength of 658 nm and a Wyatt Optilab T-rEX refractive index detector. The $\partial n/\partial c$ for each copolymer was calculated by a weight average of the measured refractive index increments of the constituent homopolymers.[35] SEC traces and molecular characteristics are provided in the Supporting Information.

Small-Angle X-ray Scattering/Mid-Angle X-ray Scattering. The phase behavior was determined by SAXS; mid-angle X-ray scattering (MAXS) was used to estimate the distance between backbones of the bottlebrush homopolymer. SAXS measurements were performed at beamlines 12-ID-B and 5-ID-D at the Advanced Photon Source, Argonne National Laboratory. The dry polymers were loaded into standard and TZero DSC pans for sectors 12-ID-B and 5-ID-D, respectively, and hermetically sealed under argon. To erase any thermal history, the samples were annealed in an oven at 140 °C for 24 h and then slowly cooled to room temperature. Samples for SAXS were heated and cooled at 10 °C/min and examined at five different temperatures between 24 and 200 °C. At each temperature, the samples were annealed for 15 min prior to exposure for 1 s, and two-dimensional (2D) SAXS patterns were obtained. At sector 12-ID-B, the X-ray wavelength was λ = 0.886 Å, at a sample-to-detector distance of 3.6 m, which provided a scattering wavevector $[q = 4\pi\lambda^{-1}\sin(\theta/2)]$ range of 2.24×10^{-3} to 0.0896 Å^{-1}. At sector 5-ID-D, the X-ray wavelength was 0.729 Å, and the sample-to-detector distance was 8.5 m, providing a q range of 2.35×10^{-3} to 0.192 Å^{-1}. MAXS data were collected at a sample-to-detector distance of 1.01 m, which gives a q range of 0.13−0.86 Å^{-1}. The isotropic 2D patterns were azimuthally averaged to obtain one-dimensional (1D) scattering intensity as a function of q. The SAXS data were analyzed with IGOR Pro (WaveMetrics, Inc.) software using a SAXS indexing macro.[36] Further analysis has been carried out using OriginLab software. The fitting of the domain spacing has been performed by the default nonlinear fitting function.

Differential Scanning Calorimetry. The glass transition temperature (T_g) of selected block polymers and homopolymers was determined by DSC. For each sample, 5−10 mg of the dry polymer was loaded into TZero aluminum pans and the samples were initially heated from 40 to 160 °C at a heating rate of 10 °C/min to eliminate the effects of thermal history. The samples were then cooled to −180 °C and heated to 200 °C at 10 °C/min; this second heating cycle was used to determine the T_g of the polymers. DSC data for the homopolymers and block polymers are provided in Figures S31 and S32 in the Supporting Information.

Rheology. Small-amplitude oscillatory shear (SAOS) experiments were used to estimate the statistical segment length of E, M, P_3, P_4, and P_9 homopolymers (see below) from the plateau modulus (G_N), using an ARES G2 rheometer (TA Instruments, Inc.), with parallel plate fixtures (8 or 25 mm diameter). Bulk homopolymer samples were loaded onto the plates and heated to 170 °C under nitrogen to inhibit polymer degradation. To remove any trapped bubbles from the sample, the polymer was subjected to steady shear. Next, the linear viscoelastic regime was determined by a strain sweep experiment at 170 °C. To identify G_N, frequency sweep experiments were performed at discrete temperatures upon cooling in the linear viscoelastic regime at frequencies and strains within the range of 0.1−100 rad/s and 1−10%, respectively. The value of G_N for each homopolymer was determined by Van Gurp-Palmen analysis of the isothermal frequency sweep, where G_N is identified as the minimum in a plot of phase angle

https://doi.org/10.1021/acs.macromol.2c00337
Macromolecules 2022, 55, 2821−2831

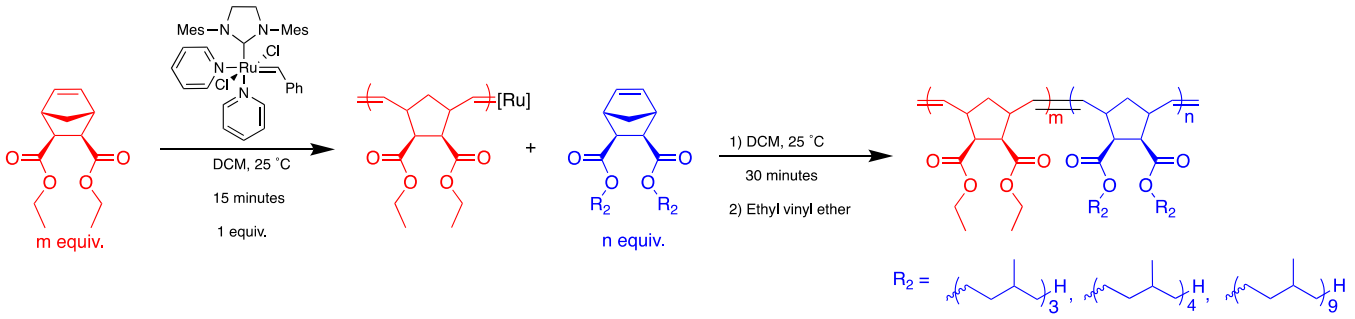

Figure 1. Sequential ROMP synthetic scheme for the preparation of EP_n-type linear-bottlebrush diblock polymers.

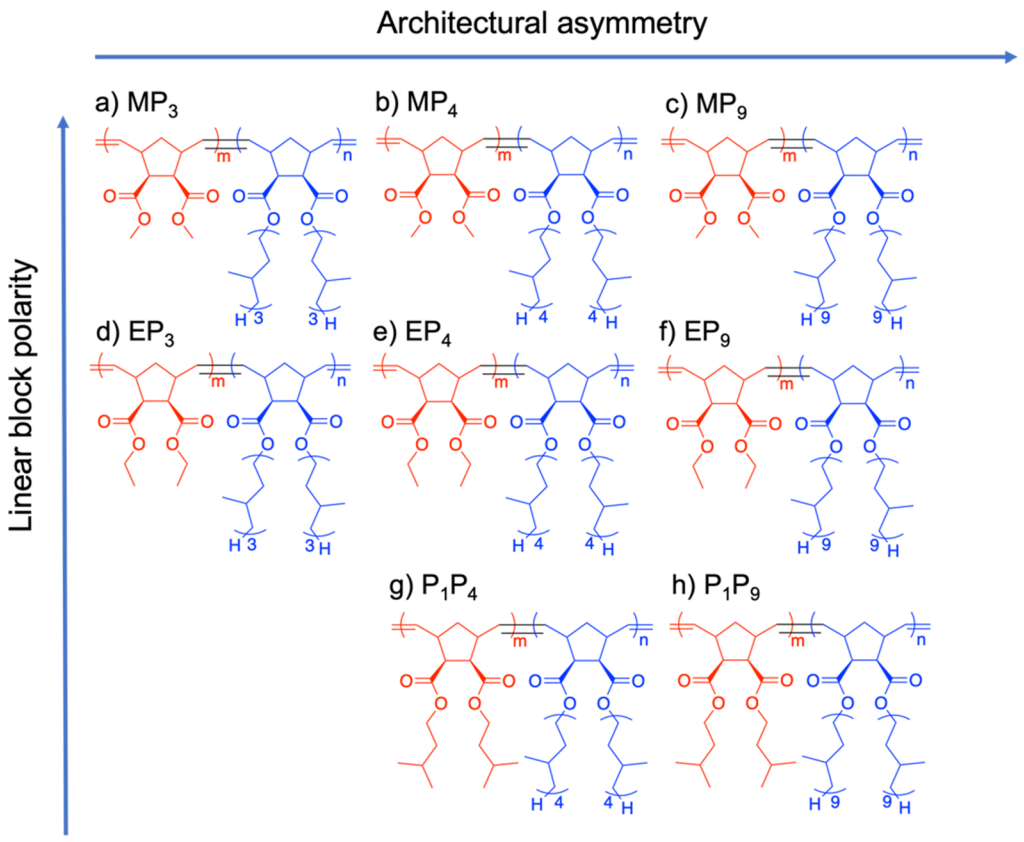

Figure 2. Schematic of the eight families of norbornene-based linear-brush block polymers, synthesized to assess the impact of architectural and chemical differences between the linear and bottlebrush blocks. (a) Poly(norbornene *exo,exo*-dimethyl ester)-*b*-poly(norbornene *exo,exo*-di-hexahydrofarnesyl ester) (MP_3). (b) Poly(norbornene *exo,exo*-dimethyl ester)-*b*-poly(norbornene *exo,exo*-di-dihydrophytyl ester) (MP_4). (c) Poly(norbornene *exo,exo*-dimethyl ester)-*b*-poly(norbornene *exo,exo*-di-perhydrosolanesyl ester) (MP_9). (d) Poly(norbornene *exo,exo*-diethyl ester)-*b*-poly(norbornene *exo,exo*-di-hexahydrofarnesyl ester) (EP_3). (e) Poly(norbornene *exo,exo*-diethyl ester)-*b*-poly(norbornene *exo,exo*-di-dihydrophytyl ester) (EP_4). (f) Poly(norbornene *exo,exo*-diethyl ester)-*b*-poly(norbornene *exo,exo*-di-perhydrosolanesyl ester) (EP_9). (g) Poly(norbornene *exo,exo*-di-isoamyl ester)-*b*-poly(norbornene *exo,exo*-di-dihydrophytyl ester) (P_1P_4). (h) Poly(norbornene *exo,exo*-di-isoamyl ester)-*b*-poly(norbornene *exo,exo*-di-perhydrosolanesyl ester) (P_1P_9).

(δ) versus complex modulus (G^*). Van Gurp-Palmen plots and information about estimates of the homopolymer statistical segment lengths are provided in the Supporting Information.

RESULTS

To study the phase behavior of linear-brush diblocks polymers with variable architectural asymmetry, we used ROMP (Figure 1) to synthesize eight types of diblock copolymers (Figure 2). Three different brush blocks were evaluated: poly(norbornene *exo,exo*-di-hexahydrofarnesyl ester), poly(norbornene *exo,exo*-di-dihydrophytyl ester), and poly(norbornene *exo,exo*-di-perhydrosolanesyl ester), abbreviated as P_3, P_4, and P_9, respectively. These were combined with three linear blocks: poly(norbornene *exo,exo*-diethyl ester), poly(norbornene *exo,exo*-dimethyl ester), and poly(norbornene *exo,exo*-di-isoamyl ester), abbreviated as, E, M, and P_1. The eight resulting diblock copolymer families, depicted in Figure 2, are EP_3, EP_4, EP_9, MP_3, MP_4, MP_9, P_1P_4, and P_1P_9. Within each family, we have varied the total degree of polymerization (N) from 91 to 511 and the volume fraction of the linear block (f_{lin}) from 0.36 to 0.8, chosen to expose the double-gyroid network morphology windows; samples are identified, for example, as $EP_3(f_{lin},N)$. ROMP provided precise control over all the molecular variables while generating low-molecular-weight dispersities ($Đ \leq 1.07$). A

https://doi.org/10.1021/acs.macromol.2c00337
Macromolecules 2022, 55, 2821−2831

complete listing of the molecular and thermal characteristics of the 258 synthesized polymers is provided in the Supporting Information.

We examined the polymers by SAXS to map the self-assembled morphologies as a function of f_{lin}, N, and temperature. Figure 3 shows representative SAXS data from

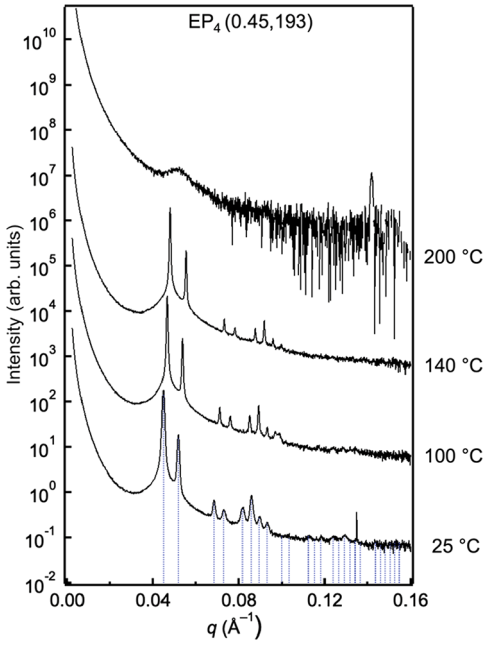

Figure 3. Vertically shifted representative 1D SAXS patterns for a double gyroid forming $EP_4(0.45,193)$ polymer as a function of temperature. Vertical lines indicate allowed reflections for double gyroid.

$EP_4(0.45,193)$ obtained between 25 and 200 °C. At 25 °C, the sharp Bragg peaks are precisely accounted for by $Ia\bar{3}d$ space group symmetry, indicative of the double-gyroid network phase. This scattering pattern persists up to 140 °C but transforms to a single broad, weak, reflection at 200 °C, consistent with a state of disorder. Figure 4 shows SAXS results for seven EP_3 polymers spanning the composition range $0.39 \leq f_{lin} \leq 0.49$ at 100 °C. These data evidence the sequence of hexagonally packed cylinders (HEX), double gyroid (GYR), and lamellae (LAM) with increasing volume fraction of the linear block. Also apparent is phase coexistence at several of the compositions near the phase boundaries, based on multiple sets of scattering reflections. A plethora of SAXS data, obtained from many of the diblock copolymers, along with representative peak indexing are provided in Figures S34−S41 in the Supporting Information.

Impact of Architectural Asymmetry. We compare the overall phase behavior of the EP_3, EP_4, and EP_9 polymers to gain an understanding of the impact of varying the linear-brush architectural asymmetry. Changing the brush block from P_3 to P_4 and then to P_9, while keeping the repeat unit structure of the linear E block invariant, increases the architectural asymmetry, that is, the space-filling characteristics of the brush blocks. We have constructed phase maps based on the SAXS data acquired across the different polymer block characteristics and over the temperature range of 25−200 °C. To facilitate the comparisons across systems, the volumetric degree of polymerization, N, defined as

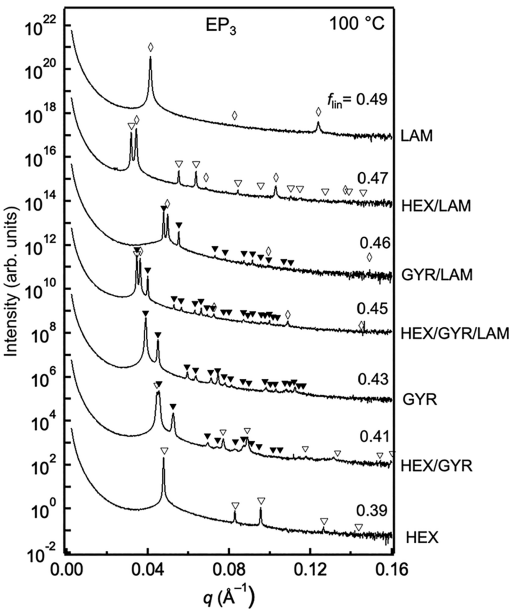

Figure 4. Vertically shifted representative 1D SAXS patterns for EP_3 polymers at 100 °C as a function of linear-block volume fractions (0.39−0.49). HEX, GYR, and LAM denote hexagonally packed cylinders, double gyroid, and lamellar ordering, respectively. Empty triangles, full triangles, and empty diamonds above the peaks indicate indexing to hexagonal, double-gyroid, and lamellar phases, correspondingly.

$$N = \left(\frac{M_n}{\rho_{lin} f_{lin} + \rho_{brush} f_{brush}}\right)\frac{1}{N_{av} v_{ref}} \quad (1)$$

has been normalized by the data acquisition temperature T, where M_n is the number-average molecular weight, ρ is the density of the constituent homopolymers, f is the volume fraction of each block, N_{av} is Avogadro's number, and the reference volume v_{ref} is chosen as 118 Å^3. N/T is proportional to χN, where χ is the Flory−Huggins segment−segment interaction parameter, typically represented as[37]

$$\chi = \frac{A}{T} + B \quad (2)$$

where A is the enthalpic term and B accounts for excess entropy.

Figure 5 illustrates the collective results for the EP_3, EP_4, and EP_9 families of linear-brush diblock copolymers. All three exhibit gyroid-containing phase windows (emphasized by pink shading) with similar widths in composition ($\Delta f_{lin} \approx 0.06$). Increasing the architectural asymmetry shifts the gyroid window to higher f_{lin}, and increasing the brush block side-chain length from P_4 to P_9 (Figure 5b,c) moves the order-to-disorder transitions (ODTs) to lower N/T. Whereas T_{ODT} values are accessible across many of the EP_3 and EP_4 polymers, none occurred within the experimental temperature range for the EP_9 materials, that is, $T_{ODT} > 200$ °C. Inaccessibility of the ODT implies stronger segregation, which retards the polymer ordering kinetics. For a given thermal treatment, this sets an upper limit on the degree of polymerization accessible to gyroid formation, which consequentially limits the accessible gyroid unit cell dimensions. This kinetic constraint might be mitigated by solvent casting, an approach to be explored in future work.

To establish how the linear-brush architecture and architectural asymmetry affect the domain spacing, we focus on the lamellae-forming samples. The backbone degree of polymer-

https://doi.org/10.1021/acs.macromol.2c00337
Macromolecules 2022, 55, 2821−2831

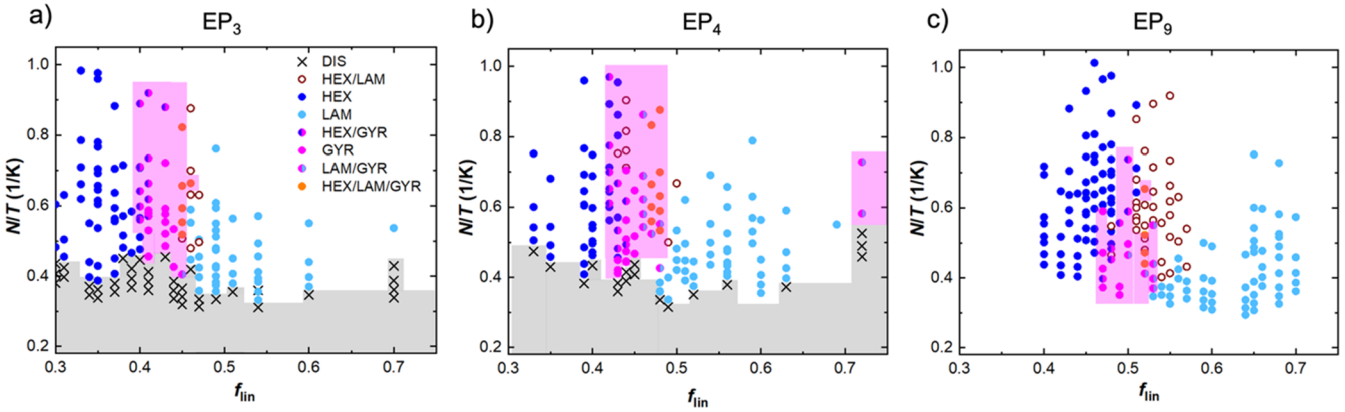

Figure 5. Phase portraits determined by SAXS for (a) EP_3, (b) EP_4, and (c) EP_9. N and T (ordinate) refer to the volumetric degree of polymerization and the SAXS measurement temperature in Kelvin, respectively; f_{lin} (abscissa) is the volume fraction of the linear block. DIS, HEX, GYR, and LAM in the legend denote disorder, hexagonally packed cylinders, double gyroid, and lamellae, respectively. The pink window identifies the double-gyroid-containing window, while the gray region represents the disordered state.

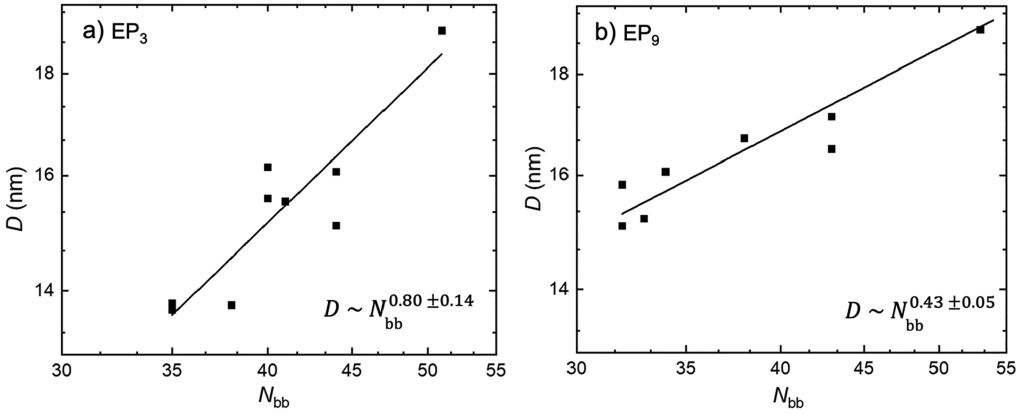

Figure 6. Scaling of lamellar domain spacing (D) with polymer backbone degree of polymerization (N_{bb}) for (a) EP_3 and (b) EP_9. The errors in N_{bb} and D are ∼10 and 3%, respectively. The axes are on logarithmic scales.

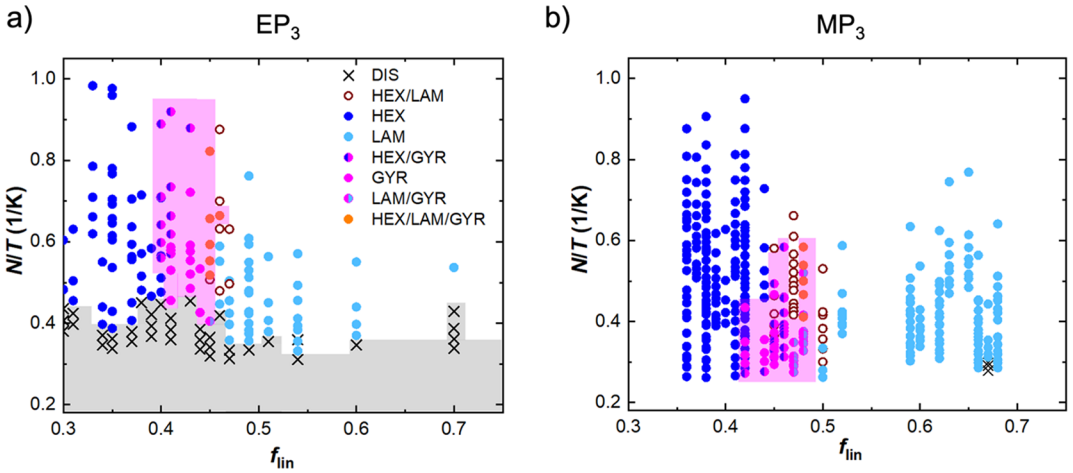

Figure 7. Phase portraits determined by SAXS for (a) EP_3 and (b) MP_3. N and T on the abscissa refer to the volumetric degree of polymerization and the temperature in Kelvin, respectively; f_{lin} on the ordinate is the volume fraction of the linear block. DIS, HEX, GYR, and LAM on the legend denote disorder, hexagonally packed cylinders, double gyroid, and lamellae, respectively. The pink window shows the double-gyroid window, while the gray region represents the disordered state.

ization (N_{bb}) was determined from a combination of ^{1}H NMR spectroscopy and SEC-MALS (see the Supporting Information), and the domain spacing (D) was calculated as $D = 2\pi/q^*$, where q^* represents the primary peak position. Figure 6 shows plots of D versus N_{bb} for the two limiting cases of architectural asymmetry, EP_3 and EP_9 (Figure 6a,b). By fitting the data to a power law, we find two distinct scaling behaviors: for EP_3, the scaling is $D \sim N_{bb}^{0.80\pm0.14}$, while EP_9 is characterized by the much weaker power law $D \sim N_{bb}^{0.43\pm0.05}$ (the error is the standard deviation of the nonlinear fit of the power of N_{bb}). For linear–

https://doi.org/10.1021/acs.macromol.2c00337
Macromolecules 2022, 55, 2821−2831

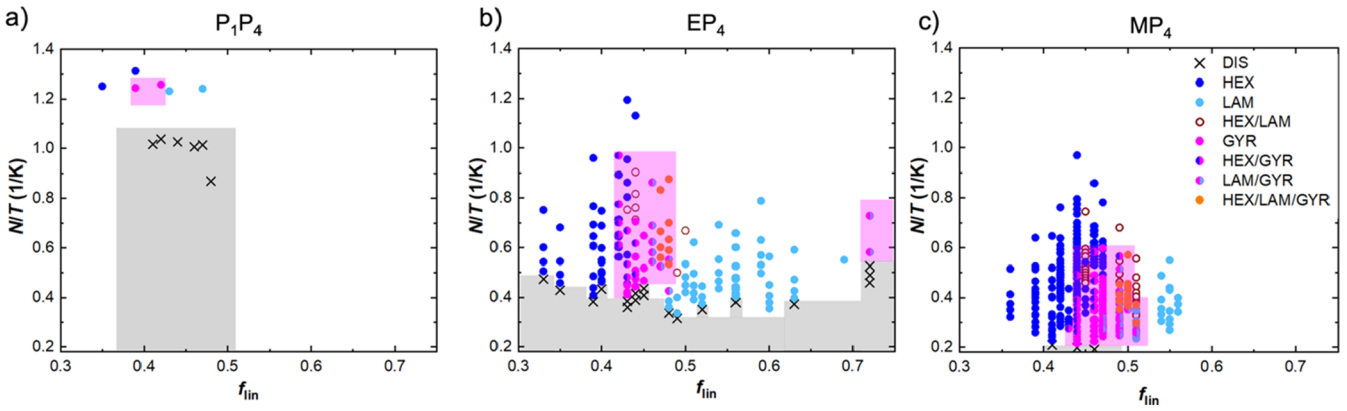

Figure 8. Phase portraits determined by SAXS for (a) P_1P_4, (b) EP_4, and (c) MP_4. N and T refer to the volumetric degree of polymerization and the SAXS measurement temperature in Kelvin, respectively; f_{lin} is the volume fraction of the linear block. DIS, HEX, GYR, and LAM denote disorder, hexagonally packed cylinders, double gyroid, and lamellae, respectively. The pink window identifies the double-gyroid window, while the gray region represents the disordered state.

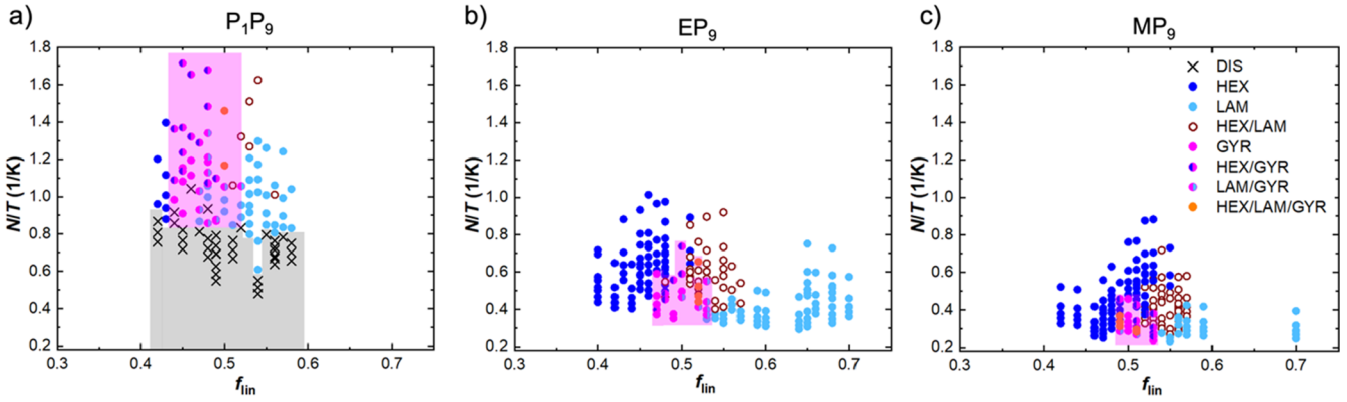

Figure 9. Phase portraits determined by SAXS for (a) P_1P_9, (b) EP_9, and (c) MP_9. N and T refer to the volumetric degree of polymerization and the SAXS measurement temperature in Kelvin, respectively; f_{lin} is the volume fraction of the linear block. DIS, HEX, GYR, and LAM on the legend denote disorder, hexagonally packed cylinders, double gyroid, and lamellae, respectively. The pink window identifies the double-gyroid window, while the gray region represents the disordered state.

linear diblock copolymers, the scaling behavior in the strong segregation limit is predicted to be $D \sim N^{2/3}$,[34] a result that has been confirmed by numerous experiments.[38−42] Within the experimental error, the EP_3 polymers conform to the conventional scaling, while for EP_9, the scaling exponent of 0.43 ± 0.05 lies well below 2/3. This indicates that at high architectural asymmetries, the domain spacing for lamellae-forming polymers deviates from the strong segregation limit prediction for linear polymers. A possible explanation for this observation is presented below. Equivalent analysis performed for cylinder-forming EP_3 and EP_9 polymers (Figure S42) reveals that both sets of polymers exhibit a behavior close to that for EP_3 lamellae and to the classical scaling of linear diblocks in the strong segregation limit (see the Supporting Information for discussion).

Linear Versus Brush Block Structure. The role of the linear block structure was probed by varying the R_1 group (Figure 1) between C_1, C_2, and C_5, in combination with the P_3, P_4, and P_9 brush side chains (Figure 2). Figure 7 shows the phase portraits obtained for EP_3 and MP_3, Figure 8 compares the results for P_1P_4, EP_4, and MP_4, and Figure 9 depicts the phase behavior for P_1P_9, EP_9, and MP_9. In each of these figures, the phase portraits are sequenced from left to right with increasing cohesive energy density ("polarity") of the linear block, for example, the methyl ester-based repeat unit (M) has a higher polarity than the ethylene−propylene (P_1) repeat unit due to a greater oxygen-to-carbon ratio. As the polarity of the linear block increases, the phase boundaries systematically shift to lower N/T values, indicative of increasing segregation strength.

Figures 8 and 9 also indicate that linear-block polarity modulates the size of the double-gyroid window. Computational work by Cochran et al.,[17] which examined the stability window of the double gyroid in linear−linear diblock copolymers in the strong segregation limit, predicts that at low segregation strengths, the double-gyroid window is narrow in composition and then expands as the segregation strength increases, but beyond a critical value of χN, the window slightly shrinks again. This means that there is a range of optimal segregation strengths where the window is the widest. In our data, we observe this effect by tuning the linear-block polarity. For P_1P_4 diblocks, the segregation strength is barely high enough to capture ordered phases at the lowest experimental temperatures (Figure 8a), and the double-gyroid window appears to be narrow ($\Delta f \approx 0.03$). For EP_4 and MP_4, the increase in linear block polarity increases the segregation strength, and the gyroid windows expand to $\Delta f \approx 0.06$ and 0.08, respectively (Figure 8b,c). Figure 9 shows that for P_1P_9, the size of the window is about 0.08 (Figure 9a) but narrows to 0.06 for EP_9 and 0.04 for MP_9 (Figure 9b,c, respectively), as the segregation strength increases.

https://doi.org/10.1021/acs.macromol.2c00337
Macromolecules 2022, 55, 2821−2831

DISCUSSION

In this work, we systematically explore the phase behavior of linear-brush diblock polymer melts around the double-gyroid network phase window. We are able to survey a large set of molecular parameters using the highly efficient ROMP synthetic approach, which provided the opportunity to examine the effects of architectural asymmetry and the strength of interaction between the two blocks. With a set of 258 synthesized polymers, we provide experimental realization of previous SCFT predications for linear−linear and linear-brush copolymers[20,22] and contribute new insights into the behavior of architecturally asymmetric diblock copolymers.

Our results indicate that greater diblock polymer architectural asymmetry, controlled by brush side-chain length, shifts the phase boundaries toward higher linear block volume fractions, while leaving the size of the double-gyroid window largely unaffected (Figure 5). Distortion of the phase diagram has been reported based on SCFT calculations in the strong segregation limit for both architecturally and conformationally asymmetric polymers.[18,20] Furthermore, our results are in direct agreement with a recent computational report by Park et al.,[22] which focused specifically on how the stability of the double-gyroid window is affected by the side-chain length of the brush block in linear-brush diblock polymers. These SCFT calculations predict that when the linear block is in the minority domain, the increase in brush side-chain length, that is, architectural asymmetry, deflects the phase boundaries of the window to higher compositions, without affecting the width.[22] The distortion of phase boundaries has been rationalized by the overall conformational asymmetry, driven in this case by the architectural asymmetry of the linear-brush polymers. Conformational asymmetry, $\varepsilon = (b_{lin}/b_{brush})^2$, reflects the difference between how two linear flexible blocks occupy space, where $b = R_g(6/N)^{1/2}$ is the statistical segment length at a common segment volume and R_g is the radius of gyration. Introducing longer arms to the brush block perturbs b_{brush} and hence modifies ε.

Changing the brush block side-chain length also influences the amount of physical (as opposed to conformational) space occupied by the block, which impacts the free energy competition between chain stretching and segment−segment interactions that determine the ultimate morphology. What we refer to as architectural asymmetry includes both of these effects. To our knowledge, the distinction between conformational asymmetry and the volume-filling aspects associated with bottlebrush side chains has not been treated theoretically. In particular, we note that there is ambiguity in defining the χ parameter, which must be renormalized to account for inaccessible segment−segment interactions associated with the mean-field treatment due to the crowded nature of the local environment created by the bottlebrush architecture.

We have estimated ε for the eight linear-brush block polymer families by SAOS rheology of the constituent homopolymers, where b_{lin} and b_{brush}, normalized to a common reference volume, 118 Å^3, were evaluated by the plateau modulus from Van Gurp-Palmen plots,[43−45] as detailed in the Supporting Information. Estimation of b based on the plateau modulus assumes Gaussian chain statistics, which may not be accurate for bottlebrush blocks. However, to the best of our knowledge, there is no alternative analysis that captures the bottlebrush chain behavior. Therefore, although these bottlebrush b values may not be strictly valid, they should represent an internally consistent trend.

Based on the b estimates from rheology, changing the brush block from P_3 to P_9 increases the conformational asymmetry with the linear E block from 2.6 to 3.5, as listed in Table 1. High conformational asymmetry induces favorable curvature toward the linear block. At very low linear-block volume fractions, this effect has been demonstrated to drive the formation of complex spherical phases, such as Frank−Kasper A15 and σ phases.[31] In the current situation, at higher linear block volume fractions, this leads to a shift in the double-gyroid phase boundaries because of entropic considerations. As suggested by Park et al.,[22] the spontaneous curvature toward the linear block relaxes the brush blocks near the interface between the domains, while the linear blocks have to give up entropy due to stretching. This favors the formation of phases with curved interfaces, such as hexagonally packed cylinders and double gyroid, while destabilizing the lamellar phase, thereby pushing the lamellar phase boundaries toward higher volume fractions. BCP composition and molecular weight control the double-gyroid network dimensions and pore size, where the latter is determined by the brush molecular volume. Therefore, the effect that the architectural asymmetry exerts over the gyroid compositional windows could be exploited to tailor the network pore size, where higher architectural asymmetries will favor the formation of network phases with smaller pore sizes for a given block polymer molecular weight.

Table 1. Conformational Characteristics

diblock polymer	b_{lin} (Å)[a]	b_{brush} (Å)[b]	ε[c]
EP_3	5.4	3.4	2.6
EP_4	5.4	3.3	2.8
EP_9	5.4	2.9	3.5
MP_3	5.9	3.4	3.1
MP_4	5.9	3.3	3.3
MP_9	5.9	2.9	4.2
P_1P_4	4.3	3.3	1.7
P_1P_9	4.3	2.9	2.2

[a]Statistical segment length for the linear block at a constant segment volume of 118 Å^3. [b]Statistical segment length for the brush block at a constant segment volume of 118 Å^3. [c]Conformational asymmetry [$\varepsilon = (b_{lin}/b_{brush})^2$], estimated from SAOS rheology of the constituent homopolymers (see the Supporting Information).

Through analysis of the domain spacing of the lamellae-forming polymers (Figure 6), it is clear that the linear block has to adjust its conformation as a result of the asymmetry. The results indicate that scaling of the domain spacing with N_{bb} is significantly weaker with high architectural asymmetry and deviates from the strong segregation limit expectation. This can be explained by the requirement of the polymers to fill space at a uniform density in the melt state. In brush polymers, the distance between backbones is set by the molecular weight of the side chains. The distance increases with increasing side-chain molecular weight due to the increase in steric repulsion between the side chains due to crowding, as quantified by MAXS of the brush homopolymers (Figure S1). The wide peak observed in the MAXS region is indicative of the distance between the bottlebrush backbones (d_b) in the melt. For the P_3 bottlebrush, the peak appears at $q = 0.25$ Å^{-1}, corresponding to $d_b = 2.5$ nm, while for P_9, the peak is at $q = 0.17$ Å^{-1}, corresponding to $d_b = 3.7$ nm (Figure S1). This increase in brush-block backbone distance in the linear-brush diblock forces the linear block to collapse and adopts a compressed conformation to fill space at uniform

https://doi.org/10.1021/acs.macromol.2c00337
Macromolecules 2022, 55, 2821−2831

density, as suggested by the illustration in Figure 10. This change of linear block conformation results in the reduced lamellar domain spacing.

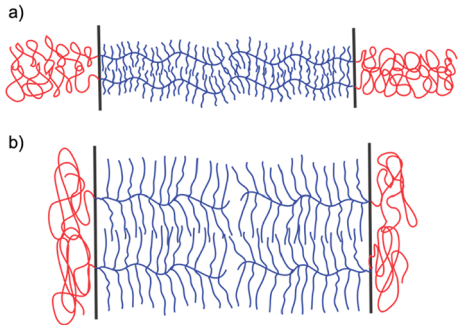

Figure 10. Schematics illustrating the proposed effect of the brush side-chain length on linear-brush packing into a lamellar phase and the lamellar domain spacing. (a,b) Illustrate packing of linear-brush polymers with short and long brush side chains, respectively.

The results from variation in linear-block identity suggest that the interaction parameter is affected by the polarity of the linear block: the order−disorder transition shifts to lower N/T values with increasing cohesive energy density (Figures 7−9). We further demonstrate that the size of the double-gyroid window is affected by the linear block polarity (Figures 8 and 9), such that there is an optimal range to provide the widest network window. To estimate how the interaction parameter is controlled by the linear block polarity, we assume the strong segregation limit. Specifically, we analyze the domain spacing of lamellar polymers for each diblock as a function of temperature (Figure 11). Note that the following treatment for the estimation of χ has been developed based on linear−linear BCPs and therefore may not be strictly appropriate in the linear-brush case. However, we use this analysis because no theoretical framework for χ has yet been developed for linear-brush diblock polymers. Therefore, the results should reflect the qualitative trends but should not be interpreted quantitatively.

In the strong segregation limit, where $\chi N \gg 10$, the linear−linear domain spacing (D) dimensions scale as[37]

$$D \sim bN^{2/3}\chi^{1/6} \tag{3}$$

where b is the average statistical segment length of the BCP, N is the total volumetric degree of polymerization, and χ is the Flory−Huggins interaction parameter. The average statistical segment length for a diblock is given by[46]

$$b = \left(\frac{1 - f_{lin}}{b_{brush}^2} + \frac{f_{lin}}{b_{lin}^2}\right)^{-0.5} \tag{4}$$

where f_{lin} is the volume fraction of the linear block, b_{lin} is the statistical segment length of the linear block, and b_{brush} is the statistical segment length of the brush block. b_{lin} and b_{brush} have been estimated from rheology (Supporting Information). For lamellar block polymers in the strong segregation limit, where $\chi N \geq 100$, the explicit expression for the lamellar domain spacing is[47]

$$D = 1.10bN^{2/3}\chi^{1/6} \tag{5}$$

χ is assumed to have a temperature dependence given by eq 2. For the highly architecturally asymmetric EP_9 and MP_9 block polymers, we incorporate the scaling behavior $D \sim N^{0.42}$ (Figure 6) instead of $D \sim N^{2/3}$, which represents the other block polymer families. By combining eqs 2, 4, and 5, plotting χ versus T^{-1} (Figure 12), and linear fitting, we have estimated A and B coefficients for all diblock types (Table 2).

When comparing between χ values for different linear blocks, while focusing on a certain brush block, we clearly see how the segregation strength increases with increasing polarity of the linear block (M > E > P_1), in agreement with the trend observed in the phase diagrams (Figures 7−9). In all cases, the excess entropy term is negative, suggesting that the linear-bottlebrush architecture favors mixing from an entropic perspective. We

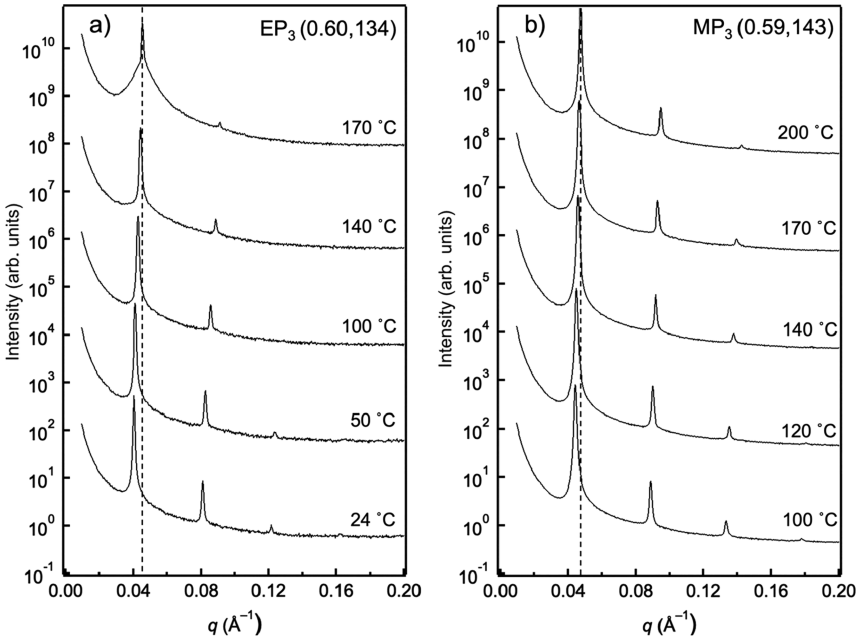

Figure 11. Vertically shifted representative 1D SAXS patterns for lamellar forming (a) EP_3(0.60,134) and (b) MP_3(0.59,143) samples as a function of temperature.

https://doi.org/10.1021/acs.macromol.2c00337
Macromolecules 2022, 55, 2821−2831

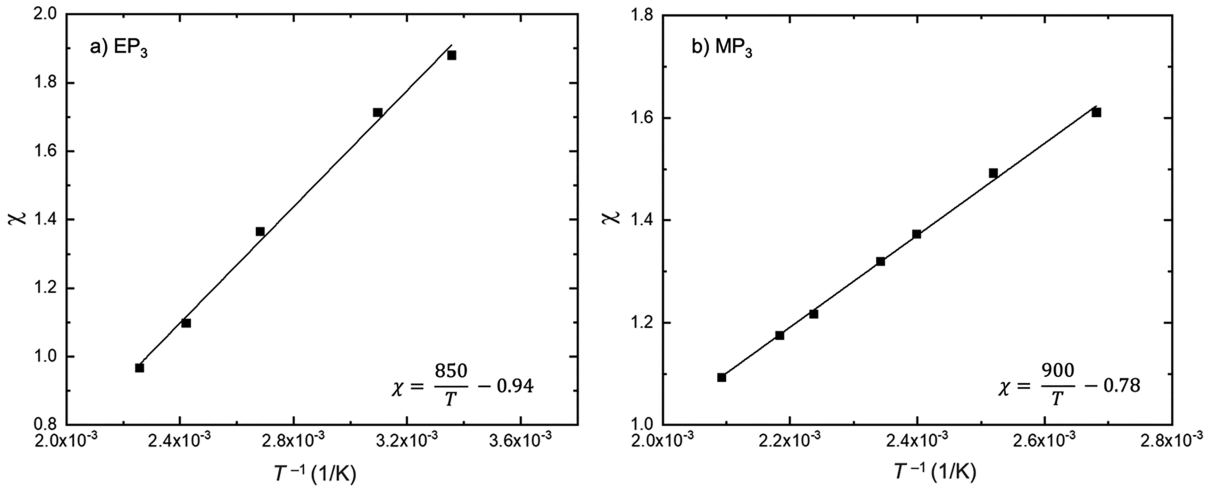

Figure 12. Estimated interaction parameter assuming strong segregation behavior for (a) EP_3 and (b) MP_3.

Table 2. Interaction Parameter for the Different Diblocks, $\chi(T) = A/T + B$, Estimated by Equations 2, 4, and 5

diblock polymer	A	B
EP_3	850	−0.94
MP_3	900	−0.78
P_1P_4	NA	NA
EP_4	700	−0.64
MP_4	1000	−0.91
P_1P_9	300	−0.20
EP_9	2.11×10^6	−836
MP_9	2.34×10^6	−724

note that the actual A and B values obtained for EP_9 and MP_9 are unreasonably high, as a result of the difference between the assumed ($N^{0.67}$) and actual scaling of D ($N^{0.42}$). Nevertheless, the significantly higher χ values explain the inaccessibility of the ODT for these polymers (Figure 9b,c). Although the obtained values should only be considered qualitatively, the trends are at least internally consistent.

Another observation from Figure 9 is that an optimal linear block polarity provides access to tunable double-gyroid network dimensions. For the P_1P_9 diblocks, the largest unit cell dimension is 58 nm obtained for N = 435. To understand whether there is any advantage of these polymers with respect to the gyroid unit cell size for a given degree of polymerization, we compare this result to dimensions reported for linear polymers in the literature. For comparison, we refer to a paper by Urbas et al.[48] where they studied the self-assembly of a high-molecular-weight linear poly(styrene-*b*-isoprene) diblock polymer in the double-gyroid morphology. They demonstrate that a 750 kg/mol (N = 11,250) polymer self-assembles into a double gyroid with a unit cell size of 258 nm. This sample is known to fall into the strong segregation limit, where $D \sim N^{2/3}$.[37] Taking this into account and calculating the expected unit cell dimensions for poly(styrene-*b*-isoprene) with N = 435, we obtain a unit cell size of 29.5 nm, which is only half the unit cell size we obtained for P_1P_9 at a comparable N. This shows that linear-brush polymers have the potential to access significantly larger unit cell dimensions than linear diblocks for a given volumetric degree of polymerization. Furthermore, the reduced entanglement of bottlebrushes should accelerate ordering kinetics relative to analogous linear−linear systems.

SUMMARY

An expansive set of 258 linear-bottlebrush diblock copolymers with variable molecular weights, compositions, architectures, and chemistries were prepared using ROMP chemistry. SAXS measurements revealed guiding rules that control the self-assembly of these architecturally asymmetric polymers into cylinders, double-gyroid, and lamellar microstructures. In qualitative agreement with previous computational studies, we demonstrate that the architectural asymmetry mainly controls the compositions over which the double-gyroid phase forms, where the phase boundaries shift toward higher linear block compositions with larger brush block side-chain lengths. This is primarily explained by the preferred curvature toward the linear block, induced by enhanced conformational asymmetry and greater space-filling character of the brush block. We also show that the domain spacing of architecturally asymmetric linear-brush diblock copolymers varies more weakly with the degree of polymerization than the documented behavior of linear−linear diblock copolymers. Furthermore, regulation of the polarity of the linear block by varying the short ligands attached to the repeat units modifies the effective interaction parameter between the linear and the brush blocks and hence the segregation strength of the architecturally asymmetric diblocks. This also influences the size of the double-gyroid window, and as expected from SCFT, at an optimal segregation strength, controlled by the linear block polarity, the window is widest.

ASSOCIATED CONTENT

Supporting Information

The Supporting Information is available free of charge at https://pubs.acs.org/doi/10.1021/acs.macromol.2c00337.

Detailed synthesis information, ^{1}H NMR spectra, SEC-MALS traces, DSC traces, SAXS, MAXS patterns, and rheology data analysis (PDF)

AUTHOR INFORMATION

Corresponding Authors

Frank S. Bates − *Department of Chemical Engineering & Materials Science, University of Minnesota, Minneapolis, Minnesota 55455, United States;* orcid.org/0000-0003-3977-1278; Email: bates001@umn.edu

Timothy P. Lodge − *Department of Chemical Engineering & Materials Science and Department of Chemistry, University of*

https://doi.org/10.1021/acs.macromol.2c00337
Macromolecules 2022, 55, 2821−2831

Minnesota, Minneapolis, Minnesota 55455, United States; orcid.org/0000-0001-5916-8834; Email: lodge@umn.edu

Authors

Lucy Liberman − *Department of Chemical Engineering & Materials Science and Department of Chemistry, University of Minnesota, Minneapolis, Minnesota 55455, United States;* orcid.org/0000-0001-9139-1163

McKenzie L. Coughlin − *Department of Chemical Engineering & Materials Science, University of Minnesota, Minneapolis, Minnesota 55455, United States;* orcid.org/0000-0001-9047-3319

Steven Weigand − *Argonne National Laboratory, Lemont, Illinois 60439, United States*

Complete contact information is available at: https://pubs.acs.org/10.1021/acs.macromol.2c00337

Notes

The authors declare no competing financial interest.

■ ACKNOWLEDGMENTS

This work was supported by the National Science Foundation through the University of Minnesota MRSEC under award number DMR-2011401. Synchrotron SAXS experiments were performed at the 12-ID-B and 5-ID-D beamlines of the Advanced Photon Source (APS). This research used resources of the Advanced Photon Source, a U.S. Department of Energy (DOE) Office of Science User Facility operated for the DOE Office of Science by Argonne National Laboratory under contract no. DE-AC02-06CH11357. We thank Dr. Aaron Lindsay for his help with the collection of rheology and DSC data, Dr. David Giles for discussion and help with rheology and DSC measurements, and Prof. Mahesh Mahanthappa for fruitful discussions.

■ REFERENCES

(1) Bates, F. S.; Fredrickson, G. H. Block Copolymers-Designer Soft Materials. *Phys. Today* **1999**, *52*, 32−38.
(2) Hamley, I. W. Block Copolymers. *Encyclopedia of Polymer Science and Technology*; Wiley, 2002; Vol. *1*.
(3) Meuler, A. J.; Hillmyer, M. A.; Bates, F. S. Ordered Network Mesostructures in Block Polymer Materials. *Macromolecules* **2009**, *42*, 7221−7250.
(4) Thomas, E. L. Nanoscale 3D Ordered Polymer Networks. *Sci. China Chem.* **2018**, *61*, 25−32.
(5) Hajduk, D. A.; Harper, P. E.; Gruner, S. M.; Honeker, C. C.; Kim, G.; Thomas, E. L.; Fetters, L. J. The Gyroid: A New Equilibrium Morphology in Weakly Segregated Diblock Copolymers. *Macromolecules* **1994**, *27*, 4063−4075.
(6) Chu, C.-Y.; Lin, W.-F.; Tsai, J.-C.; Lai, C.-S.; Lo, S.-C.; Chen, H.-L.; Hashimoto, T. Order-Order Transition between Equilibrium Ordered Bicontinuous Nanostructures of Double Diamond and Double Gyroid in Stereoregular Block Copolymer. *Macromolecules* **2012**, *45*, 2471−2477.
(7) Chu, C. Y.; Jiang, X.; Jinnai, H.; Pei, R. Y.; Lin, W. F.; Tsai, J. C.; Chen, H. L. Real-Space Evidence of the Equilibrium Ordered Bicontinuous Double Diamond Structure of a Diblock Copolymer. *Soft Matter* **2015**, *11*, 1871−1876.
(8) Chang, C. Y.; Manesi, G. M.; Yang, C. Y.; Hung, Y. C.; Yang, K. C.; Chiu, P. T.; Avgeropoulos, A.; Ho, R. M. Mesoscale Networks and Corresponding Transitions from Self-Assembly of Block Copolymers. *Proc. Natl. Acad. Sci. U.S.A.* **2021**, *118*, No. e2022275118.
(9) Takenaka, M.; Wakada, T.; Akasaka, S.; Nishitsuji, S.; Saijo, K.; Shimizu, H.; Kim, M. I.; Hasegawa, H. Orthorhombic Fddd Network in Diblock Copolymer Melts. *Macromolecules* **2007**, *40*, 4399−4402.
(10) Matsen, M. W.; Schick, M. Stable and Unstable Phases of a Diblock Copolymer Melt. *Phys. Rev. Lett.* **1994**, *72*, 2660−2663.
(11) Tyler, C. A.; Morse, D. C. Orthorhombic Fddd Network in Triblock and Diblock Copolymer Melts. *Phys. Rev. Lett.* **2005**, *94*, 208302.
(12) Matsen, M. W.; Bates, F. S. Origins of Complex Self-Assembly in Block Copolymers. *Macromolecules* **1996**, *29*, 7641−7644.
(13) Vigild, M. E.; Almdal, K.; Mortensen, K.; Hamley, I. W.; Fairclough, J. P. A.; Ryan, A. J. Transformations to and from the Gyroid Phase in a Diblock Copolymer. *Macromolecules* **1998**, *31*, 5702−5716.
(14) Dair, B. J.; Honeker, C. C.; Alward, D. B.; Avgeropoulos, A.; Hadjichristidis, N.; Fetters, L. J.; Capel, M.; Thomas, E. L. Mechanical Properties and Deformation Behavior of the Double Gyroid Phase in Unoriented Thermoplastic Elastomers. *Macromolecules* **1999**, *32*, 8145−8152.
(15) Dair, B. J.; Avgeropoulos, A.; Hadjichristidis, N.; Thomas, E. L. Mechanical Properties of the Double Gyroid Phase in Oriented Thermoplastic Elastomers. *J. Mater. Sci.* **2000**, *35*, 5207−5213.
(16) Aggarwal, S. L. Structure and Properties of Block Polymers and Multiphase Polymer Systems: An Overview of Present Status and Future Potential. *Polymer* **1976**, *17*, 938−956.
(17) Cochran, E. W.; Garcia-Cervera, C. J.; Fredrickson, G. H. Stability of the Gyroid Phase in Diblock Copolymers at Strong Segregation. *Macromolecules* **2006**, *39*, 2449−2451.
(18) Matsen, M. W.; Bates, F. S. Conformationally Asymmetric Block Copolymers. *J. Polym. Sci., Part B: Polym. Phys.* **1997**, *35*, 945−952.
(19) Matsen, M. W. Fast and Accurate SCFT Calculations for Periodic Block-Copolymer Morphologies Using the Spectral Method with Anderson Mixing. *Eur. Phys. J. E* **2009**, *30*, 361−369.
(20) Matsen, M. W. Effect of Architecture on the Phase Behavior of AB-Type Block Copolymer Melts. *Macromolecules* **2012**, *45*, 2161−2165.
(21) Matsen, M. W.; Schick, M. Microphases of a Diblock Copolymer with Conformational Asymmetry. *Macromolecules* **1994**, *27*, 4014−4015.
(22) Park, S. J.; Cheong, G. K.; Bates, F. S.; Dorfman, K. D. Stability of the Double Gyroid Phase in Bottlebrush Diblock Copolymer Melts. *Macromolecules* **2021**, *54*, 9063−9070.
(23) Grason, G. M.; Kamien, R. D. Interfaces in Diblocks: A Study of Miktoarm Star Copolymers. *Macromolecules* **2004**, *37*, 7371−7380.
(24) Li, W.; Liu, Y. X. Simplicity in Mean-Field Phase Behavior of Two-Component Miktoarm Star Copolymers. *J. Chem. Phys.* **2021**, *154*, 014903.
(25) Li, Z.; Tang, M.; Liang, S.; Zhang, M.; Biesold, G. M.; He, Y.; Hao, S.-M.; Choi, W.; Liu, Y.; Peng, J.; Lin, Z. Bottlebrush Polymers: From Controlled Synthesis, Self-Assembly, Properties to Applications. *Prog. Polym. Sci.* **2021**, *116*, 101387.
(26) Verduzco, R.; Li, X.; Pesek, S. L.; Stein, G. E. Structure, Function, Self-Assembly, and Applications of Bottlebrush Copolymers. *Chem. Soc. Rev.* **2015**, *44*, 2405−2420.
(27) Kawamoto, K.; Zhong, M.; Gadelrab, K. R.; Cheng, L.-C.; Ross, C. A.; Alexander-Katz, A.; Johnson, J. A. Graft-through Synthesis and Assembly of Janus Bottlebrush Polymers from A-Branch-B Diblock Macromonomers. *J. Am. Chem. Soc.* **2016**, *138*, 11501−11504.
(28) Guo, Z. H.; Le, A. N.; Feng, X.; Choo, Y.; Liu, B.; Wang, D.; Wan, Z.; Gu, Y.; Zhao, J.; Li, V.; Osuji, C. O.; Johnson, J. A.; Zhong, M. Janus Graft Block Copolymers: Design of a Polymer Architecture for Independently Tuned Nanostructures and Polymer Properties. *Angew. Chem., Int. Ed.* **2018**, *57*, 8493−8497.
(29) Jiang, L.; Nykypanchuk, D.; Pastore, V. J.; Rzayev, J. Morphological Behavior of Compositionally Gradient Polystyrene-Polylactide Bottlebrush Copolymers. *Macromolecules* **2019**, *52*, 8217−8226.
(30) Mueller, A. J.; Lindsay, A. P.; Jayaraman, A.; Lodge, T. P.; Mahanthappa, M. K.; Bates, F. S. Quasicrystals and Their Approximants

in a Crystalline-Amorphous Diblock Copolymer. *Macromolecules* **2021**, *54*, 2647−2660.
(31) Chang, A. B.; Bates, F. S. Impact of Architectural Asymmetry on Frank-Kasper Phase Formation in Block Polymer Melts. *ACS Nano* **2020**, *14*, 11463−11472.
(32) Chang, A. B.; Lin, T.-P.; Thompson, N. B.; Luo, S.-X.; Liberman-Martin, A. L.; Chen, H.-Y.; Lee, B.; Grubbs, R. H. Design, Synthesis, and Self-Assembly of Polymers with Tailored Graft Distributions. *J. Am. Chem. Soc.* **2017**, *139*, 17683−17693.
(33) Xia, Y.; Kornfield, J. A.; Grubbs, R. H. Efficient Synthesis of Narrowly Dispersed Brush Polymers via Living Ring-Opening Metathesis Polymerization of Macromonomers. *Macromolecules* **2009**, *42*, 3761−3766.
(34) Lin, T.-P.; Chang, A. B.; Chen, H.-Y.; Liberman-Martin, A. L.; Bates, C. M.; Voegtle, M. J.; Bauer, C. A.; Grubbs, R. H. Control of Grafting Density and Distribution in Graft Polymers by Living Ring-Opening Metathesis Copolymerization. *J. Am. Chem. Soc.* **2017**, *139*, 3896−3903.
(35) Medrano, R.; Laguna, M. T. R.; Saiz, E.; Tarazona, M. P. Analysis of Copolymers of Styrene and Methyl Methacrylate Using Size Exclusion Chromatography with Multiple Detection. *Phys. Chem. Chem. Phys.* **2003**, *5*, 151−157.
(36) Lindsay, A. P.; Mueller, A. J.; Mahanthappa, M. K.; Lodge, T. P.; Bates, F. S. *1D SAXS Indexing Macro for Igor Pro*. 2021.
(37) Bates, F. S.; Fredrickson, G. H. Block Copolymer Thermodynamics: Theory and Experiment. *Annu. Rev. Phys. Chem.* **1990**, *41*, 525−557.
(38) Hashimoto, T.; Yamasaki, K.; Koizumi, S.; Hasegawa, H. Ordered Structure in Blends of Block Copolymers. 1. Miscibility Criterion for Lamellar Block Copolymers. *Macromolecules* **1993**, *26*, 2895−2904.
(39) Hashimoto, T. Generalized View of Molecular Weight Dependence of Microdomain Size of Block Polymers. Appraisal of Hadziioannou-Skoulios' Data on Binary Mixtures of Block Polymers. *Macromolecules* **1982**, *15*, 1548−1553.
(40) Matsushita, Y.; Mori, K.; Saguchi, R.; Nakao, Y.; Noda, I.; Nagasawa, M. Molecular Weight Dependence of Lamellar Domain Spacing of Diblock Copolymers in Bulk. *Macromolecules* **1990**, *23*, 4313−4316.
(41) Hadziioannou, G.; Skoulios, A.; Hadziioannou, G. Molecular Weight Dependence of Lamellar Structure in Styrene/Isoprene Two- and Three-Block Copolymers. *Macromolecules* **1982**, *15*, 258−262.
(42) Witten, T. A.; Leibler, L.; Pincus, P. A. Stress Relaxation in the Lamellar Copolymer Mesophase. *Macromolecules* **1990**, *23*, 824−829.
(43) Fetters, L. J.; Lohse, D. J.; Richter, D.; Witten, T. A.; Zirkel, A. Connection between Polymer Molecular Weight, Density, Chain Dimensions and Melt Viscoelastic Properties. *Macromolecules* **1994**, *27*, 4639−4647.
(44) Heimenz, P. C.; Lodge, T. P. *Polymer Chemistry*; CRC Press, 2007.
(45) Lewis, R. M.; Arora, A.; Beech, H. K.; Lee, B.; Lindsay, A. P.; Lodge, T. P.; Dorfman, K. D.; Bates, F. S. Role of Chain Length in the Formation of Frank-Kasper Phases in Diblock Copolymers. *Phys. Rev. Lett.* **2018**, *121*, 208002.
(46) Davidock, D. A.; Hillmyer, M. A.; Lodge, T. P. Mapping Large Regions of Diblock Copolymer Phase Space by Selective Chemical Modification. *Macromolecules* **2004**, *37*, 397−407.
(47) Ren, Y.; Lodge, T. P.; Hillmyer, M. A. Synthesis, Characterization, and Interaction Strengths of Difluorocarbene-Modified Polystyrene-Polyisoprene Block Copolymers. *Macromolecules* **2000**, *33*, 866−876.
(48) Urbas, A. M.; Maldovan, M.; DeRege, P.; Thomas, E. L. Bicontinuous Cubic Block Copolymer Photonic Crystals. *Adv. Mater.* **2002**, *14*, 1850−1853.

https://doi.org/10.1021/acs.macromol.2c00337
Macromolecules 2022, 55, 2821−2831